# Supplementary Information for: Evaluating GNSS-T VOD sensitivity to plant water dynamics, rainfall interception, and dew in a coniferous forest

Konstantin Schellenberg[a,b,c,*], Sinikka J. Paulus[b,d], Ronald Queck[e], David Chaparro[f], Oliver Binks[f], Maurizio Mencuccini[f,g], Sharath S. Paligi[h], Henrik Hartmann[i,j,b], Christiane Schmullius[a,k], Clémence Dubois[b], Thomas Jagdhuber[c,m]

[a] *Department of Earth Observation, Institute for Geography, Friedrich Schiller University Jena, Jena, Germany*
[b] *Max Planck Institute for Biogeochemistry, Jena, Germany*
[c] *Microwaves and Radar Institute, German Aerospace Center, Oberpfaffenhofen, Germany*
[d] *Faculty of Environment and Natural Resources, University of Freiburg, Freiburg, Germany*
[e] *Institute of Hydrology and Meteorology, Dresden University of Technology, Tharandt, Germany*
[f] *CREAF, Cerdanyola del Vallès, Barcelona, Spain*
[g] *ICREA, Barcelona, Spain*
[h] *Plant Ecology and Ecosystems Research, Albrecht von Haller Institute for Plant Sciences, University of Göttingen, Göttingen, Germany*
[i] *Julius Kühn-Institute for Forest Protection, Federal Research Institute for Cultivated Plants, Quedlinburg, Germany*
[j] *Faculty of Forest sciences and Forest Ecology, Georg-August-University Göttingen, Göttingen, Germany*
[k] *School for Climate Studies, Stellenbosch University, Stellenbosch, South Africa*
[l] *Institute of Data Science, German Aerospace Center, Jena, Germany*
[m] *Institute of Geography, University of Augsburg, Augsburg, Germany*

---

This file contains Supplementary Figures.

*Corresponding author
*Email address:* konstantin.schellenberg@uni-jena.de (Konstantin Schellenberg)

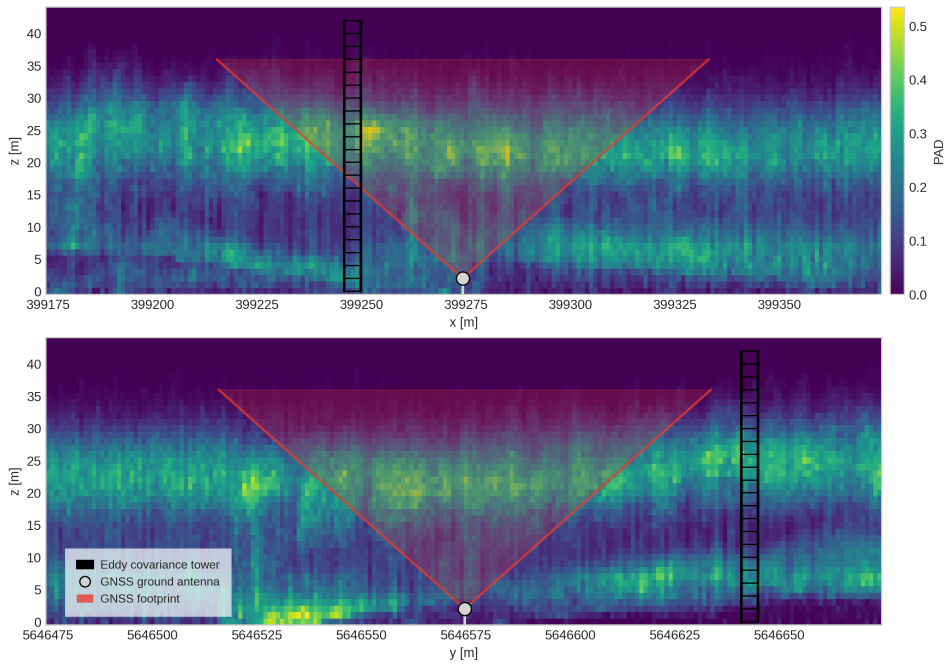


Figure S1: GNSS-T ground receiver footprint (y–x dimensions). The terrestrial laser scanning-based plant area density (PAD, $m^2\,m^{-3}$) is shown in the background to illustrate the biomass distribution at the Tharandt research site. Undergrowth is partly found in the footprint but is not abundant in the footprint itself. The eddy covariance tower is depicted in black and does not overlap with the footprint. The canopy height is calculated as the height at which 99.9% of the PAD is reached. The cutoff incidence angle for GNSS-T VOD calculations is 60°.

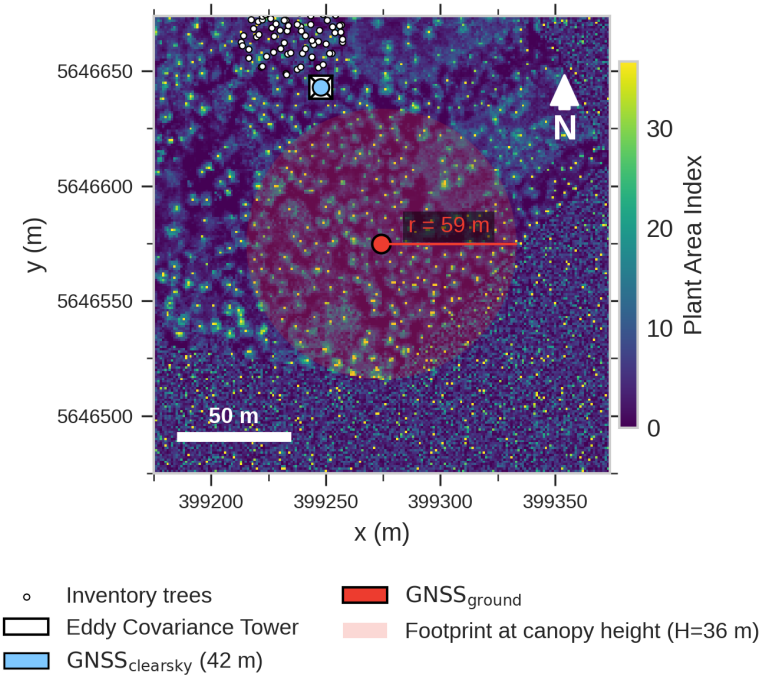


Figure S2: Similar to S1, top-down view of the GNSS-T ground receiver footprint (z-dimension).

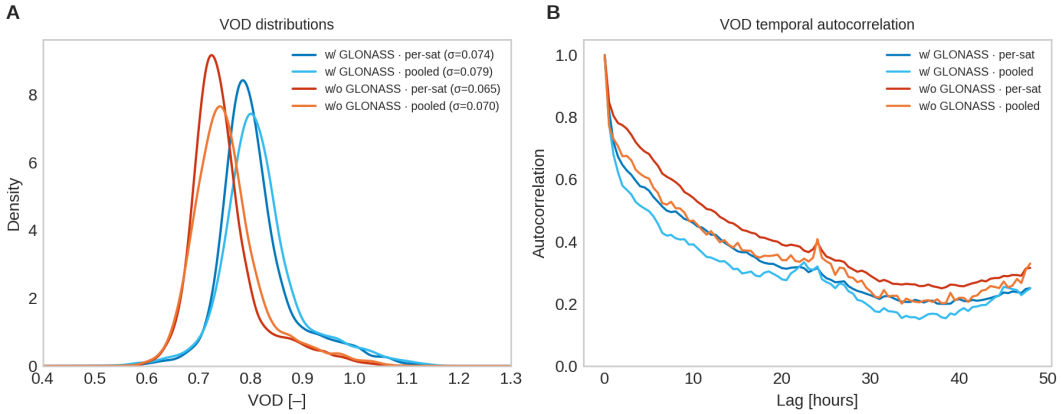


Figure S3: Comparison of the quality of GNSS-T VOD time series products calculated for including or excluding data from the GLONASS system, and by using the baseline anomaly algorithm proposed by [3] (where GLONASS and non-GLONASS systems are separate sets for the sky-sector-wise average) or satellite-wise calculations of the anomalies. The latter take the individual attenuation properties of each satellite into account. a) Distribution of 30-min VOD data, b) temporal autocorrelation. We find that removing GLONASS and choosing per-satellite anomaly calculation yields the lowest standard deviation ($\sigma$=0.065), hence, a more effective noise reduction. Simultaneously, this option shows the highest autocorrelation, indicating less correlation with noise on short time scales. Tharandt; DOY 116–366. Only incidence angles $< 60°$ are shown.

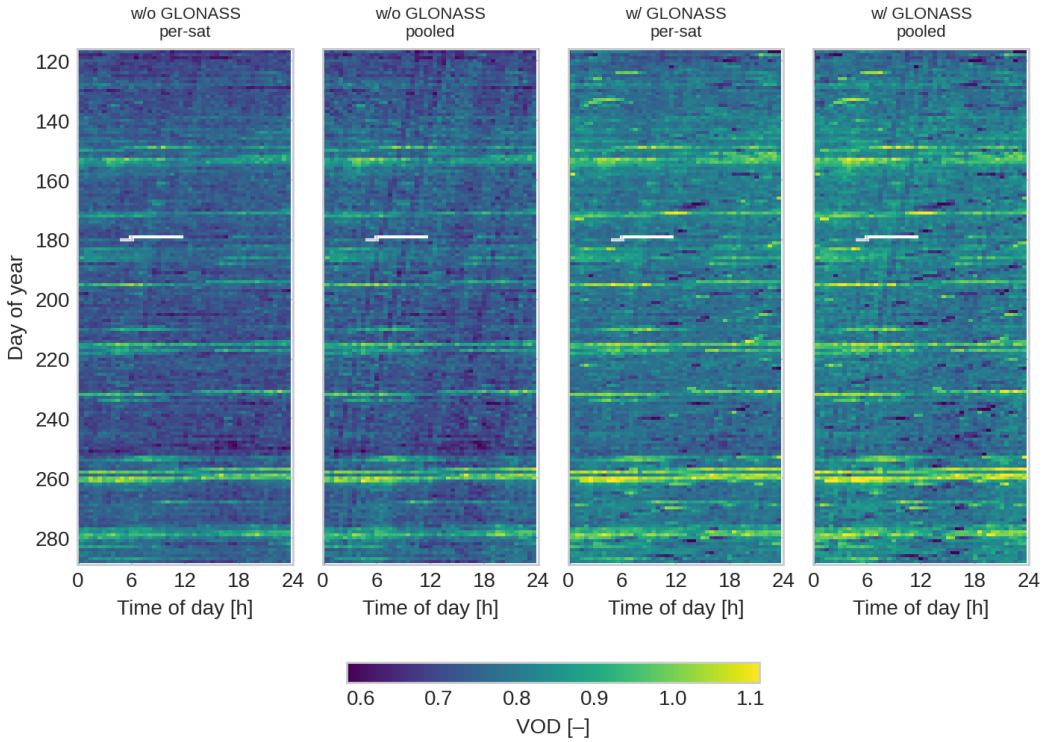


Figure S4: Temporal evolution of the GNSS-T VOD diurnal cycle. Please refer to fig. S3 for detailed description of the subplots. We observe diagonal aliases in all time series, likely orbit pattern induced that probe different parts of the inhomogeneous canopy. Excluding GLONASS and introducing satellite-wise anomaly calculation as an extension to the algorithm presented by [3] yielded a time series with least artifacts as in sudden jumps and alleviation of the aliases. Tharandt; DOY 116–366. Only incidence angles $< 60°$ are shown.

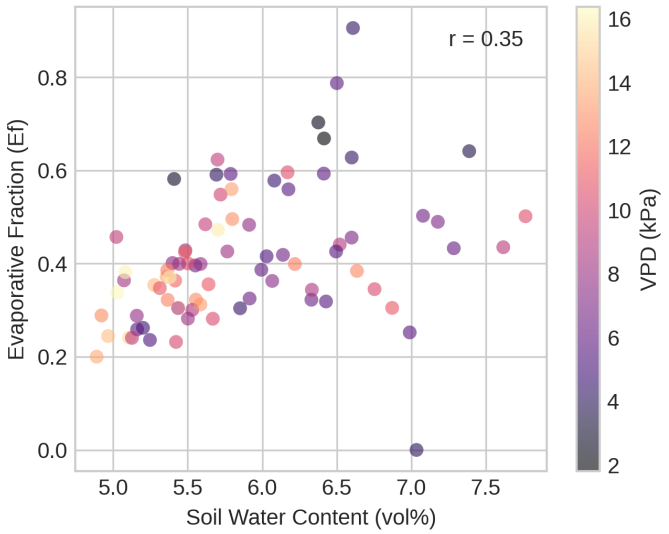


Figure S5: Indication for energy or not water limitation in the Tharandt ecosystem in 2024. The evaporative fraction (Ef=LE/Rn, latent heat flux/net Radiation) is the fraction of energy used for evaporation from all available energy. For a water limited ecosystem, a positive slope between critical soil water content and to soil wilting point is proposed while well-watered conditions show a constant ratio. We infer the inflection point between the two state of 5.5 vol% soil water content.

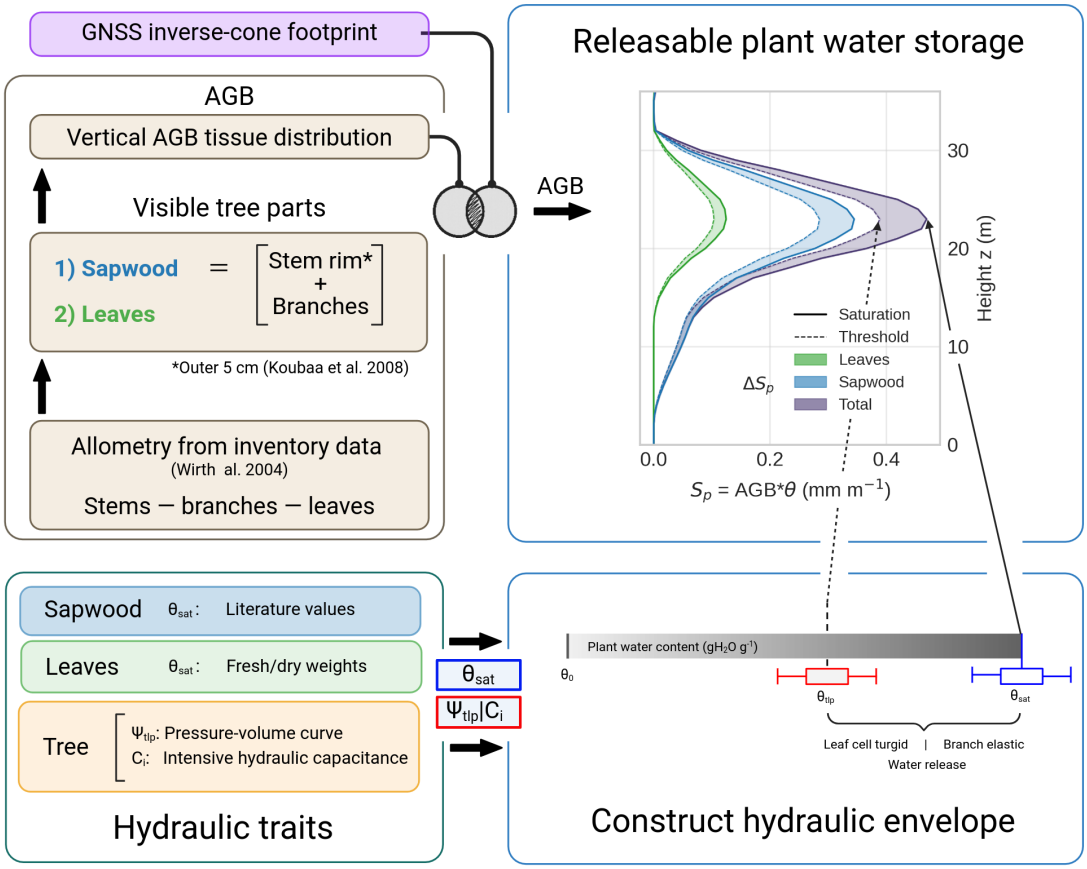


Figure S6: Workflow to calculate the maximum releasable water storage $\Delta S_p^{\max}$ from inventory data of AGB, the GNSS cone footprint, and hydraulic traits.

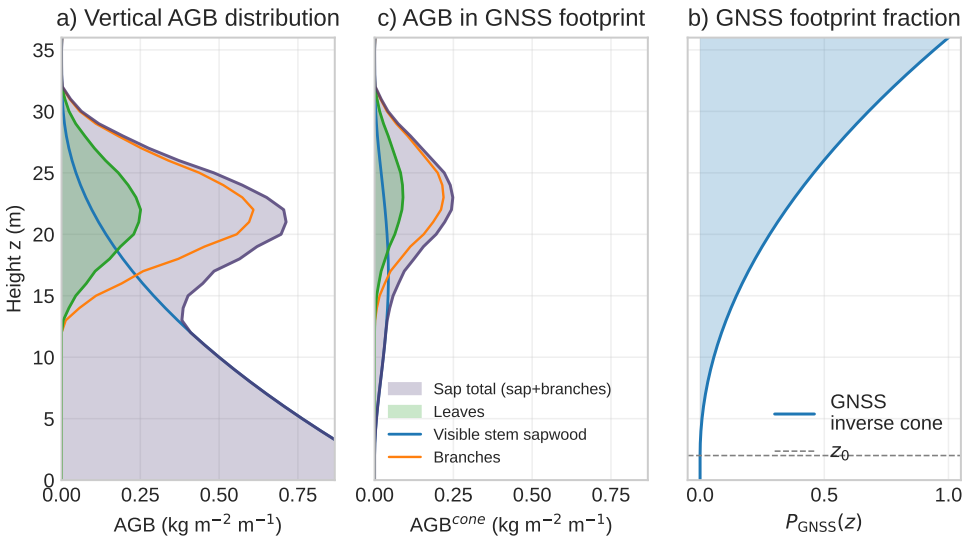


0 of 100

Figure S7: a) Above-ground biomass (AGB) of sapwood and leaves. Sapwood is the sum of branches, which are assumed to be entirely sapwood, and visible sapwood of the stem (top 2 cm). b) AGB falling into GNSS footprint. c) Fraction of canopy falling into GNSS footprint.

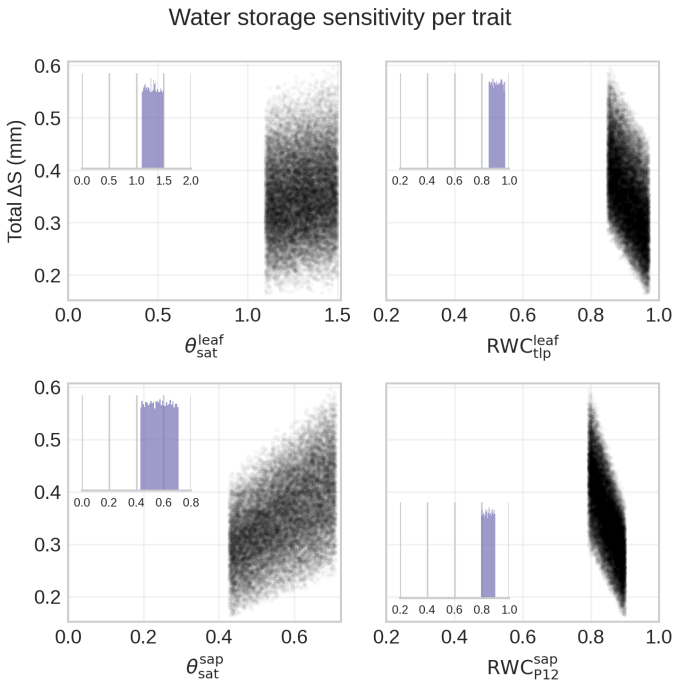


Figure S8: Monte-Carlo simulations of hydraulic traits and their effect on maximum releasable water storage $\Delta S_p$ for leaves and sapwood. We drew 20,000 random samples from an uniform trait distribution confined by the report ranges in tab. The inlet displays the prior distributions.

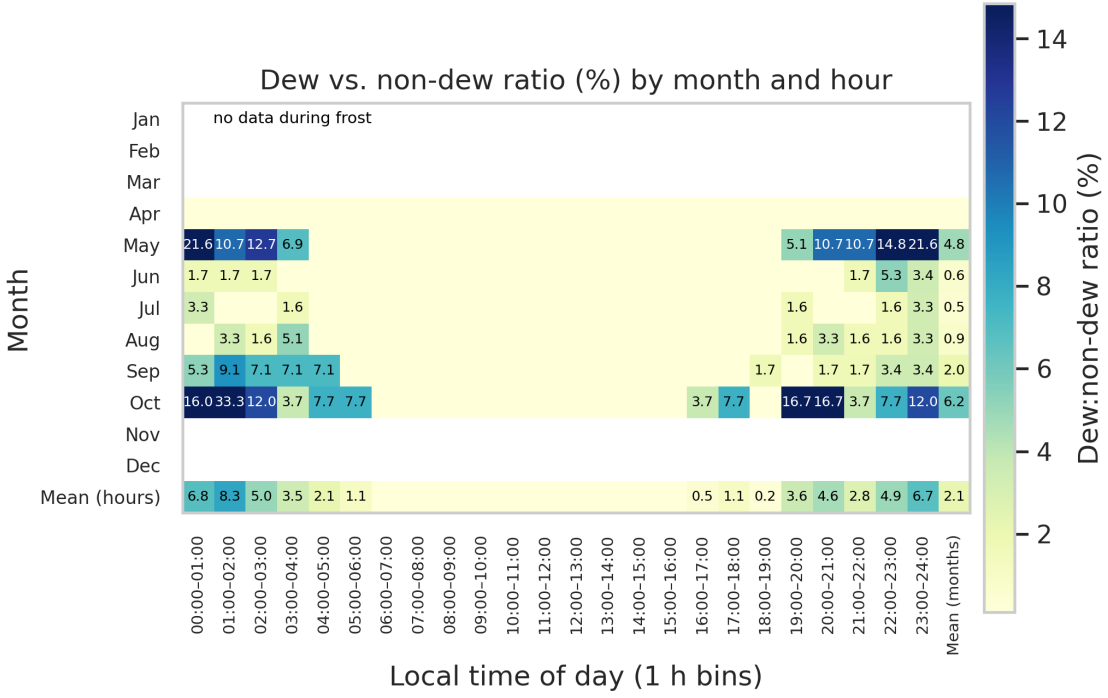


Figure S9: Dew occurrence defined by hydrometeorolgical filters at Tharandt

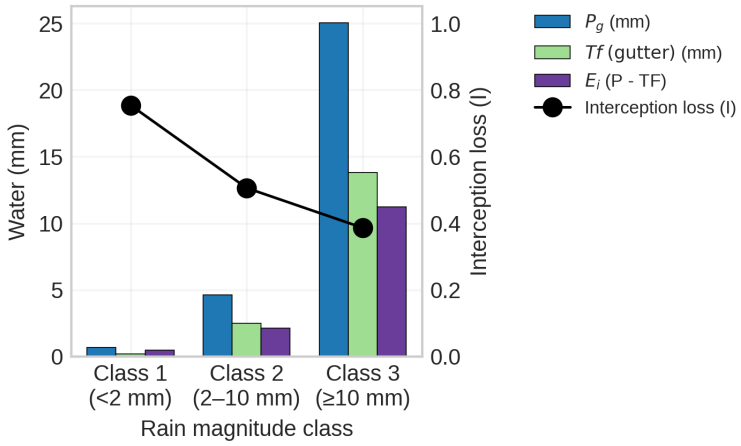


Figure S10: Interception loss per rainfall event class. Canopy influx is given as gross precipitation $P_g$, effluxes are measured throughfall $Tf$ from the collection gutter and calculated evaporation from interception from the mass balance $E_i = P_g - Tf$.

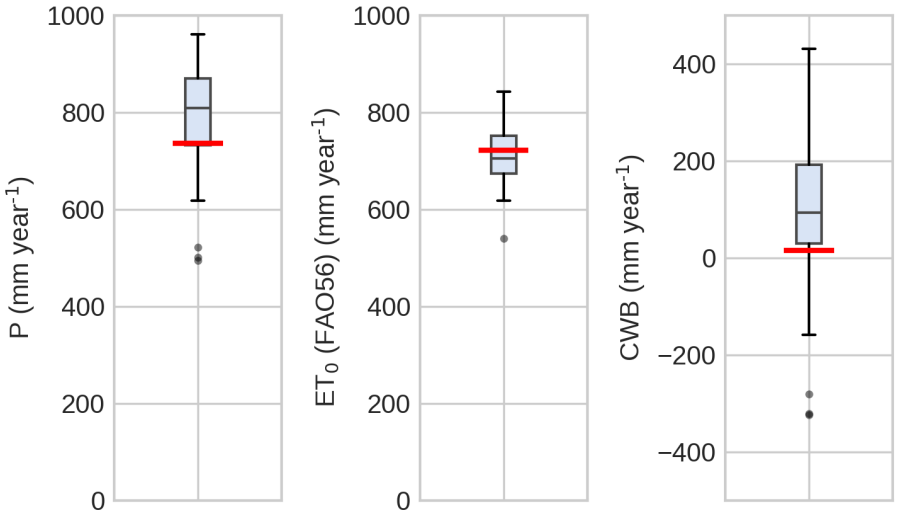


Figure S11: Comparing the climatic water balance (CWB) of the study period 2024 (marked in red) with the climatology of the preceding year (1995-2023) at Tharandt. Precipitation (left), potential evapotranspiration (middle, after FAO penmen-monteith equation for a plain grass surface [1], and CWB=P-ET$_0$. 2024 is at the 24th percentile of CWB.

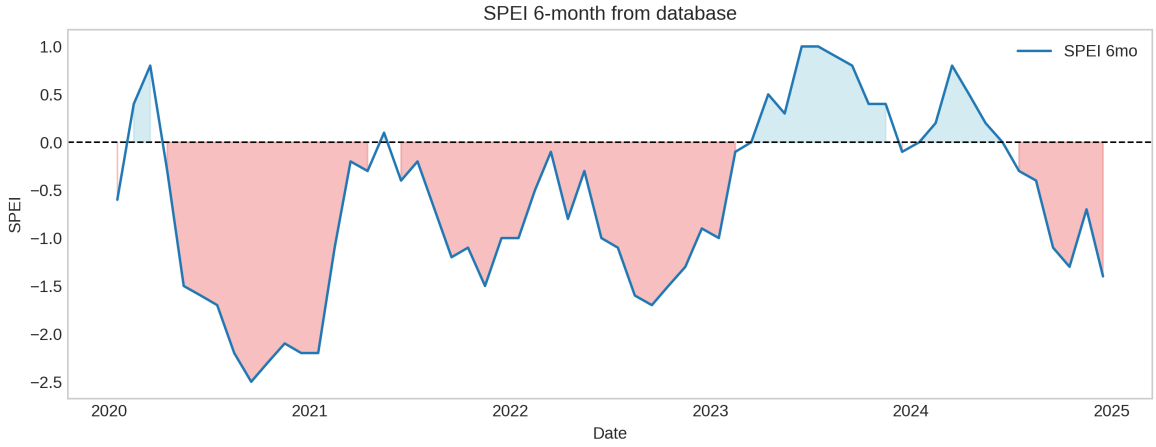


Figure S12: Standardized Precipitation Evapotranspiration Index (SPEI) with 6-month baseline of Niwot Ridge Forest research stie (US-NR1). The study period of [2] was 2022 and 2023.

## References


[1] Allen, R.G., Pruitt, W.O., Wright, J.L., Howell, T.A., Ventura, F., Snyder, R., Itenfisu, D., Steduto, P., Berengena, J., Yrisarry, J.B., Smith, M., Pereira, L.S., Raes, D., Perrier, A., Alves, I., Walter, I., Elliott, R., 2006. A recommendation on standardized surface resistance for hourly calculation of reference ETo by the FAO56 Penman-Monteith method. Agricultural Water Management 81, 1–22. URL: https://www.sciencedirect.com/science/article/pii/S037837740500154X, doi:10.1016/j.agwat.2005.03.007.

[2] Burns, S.P., Humphrey, V., Gutmann, E.D., Raleigh, M.S., Bowling, D.R., Blanken, P.D., 2025. Using GNSS-based vegetation optical depth, tree sway motion, and eddy-covariance to examine evaporation of canopy-intercepted rainfall in a subalpine forest. EGUsphere , 1–38URL: https://egusphere.copernicus.org/preprints/2025/egusphere-2025-1755/, doi:10.5194/egusphere-2025-1755. publisher: Copernicus GmbH.

[3] Humphrey, V., Frankenberg, C., 2023. Continuous ground monitoring of vegetation optical depth and water content with GPS signals. Biogeosciences 20, 1789–1811. URL: https://bg.copernicus.org/articles/20/1789/2023/, doi:10.5194/bg-20-1789-2023.